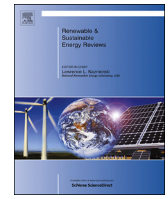
Renewable and Sustainable Energy Reviews 33 (2014) 636–644

Contents lists available at ScienceDirect

Renewable and Sustainable Energy Reviews

journal homepage: www.elsevier.com/locate/rser



Heat transfer enhancement in parabolic trough collector tube using Al_2O_3/synthetic oil nanofluid

T. Sokhansefat [a], A.B. Kasaeian [a,*], F. Kowsary [b]

[a] Department of New Sciences and Technologies, University of Tehran, Tehran, Iran
[b] School of Mechanical Engineering, University of Tehran, Tehran, Iran

A R T I C L E I N F O

Article history:
Received 21 September 2013
Received in revised form
14 January 2014
Accepted 14 February 2014
Available online 12 March 2014

Keywords:
Parabolic trough collector
Non-uniform heat flux
Monte Carlo
Nanofluid

A B S T R A C T

Three-dimensional fully developed turbulent mixed convection heat transfer of Al_2O_3/synthetic oil nanofluid in a trough collector tube with a non-uniform heat flux was numerically studied. The effect of AL_2O_3 particle concentration in the synthetic oil on the rate of heat transfer from the absorber tube was also investigated. Various nanoparticle concentrations ($<5\%$ in volume) at the operational temperatures of 300 K, 400 K, and 500 K were used in the current study. The heat flux distribution on the outer surface of the absorber tube was non-uniform in the circumferential direction but uniform in the axial direction. The heat flux in the circumferential direction was obtained using the Monte Carlo ray tracing technique. Three-dimensional Navier–Stokes mass, momentum and energy equations were solved using the FLUENT software. A second order discretization was used for the convective and diffusive terms and the SIMPLE scheme was applied for the velocity–pressure coupling. The outlet temperature of the absorber tube from the current numerical simulations was compared with existing experimental data. The absolute errors were found to be less than 3.8 °C. The current numerical results show that the convection heat transfer coefficient has a direct dependency on the volumetric concentration of nanoparticles in the fluid. In addition, the heat transfer enhancement due to the nanoparticles in the fluid reduces as the absorber operational temperature is increased.

Contents

1. Introduction

The global energy demand is increasing in an accelerating rate. Fossil fuels (oil, coal and natural gas) are currently supplying over 90% of the world's energy demands. The fossil fuels are non-renewable and limited in supplying energy indefinitely. These energy resources will eventually be depleted. In addition, combustion of fossil fuels makes carbon dioxide emission, which is one of the greenhouse gases contributing to global warming. Use of renewable energy resources, on the other hand, can lead to reduction in fossil fuel consumption and in turn protection of the environment. Solar energy is one of the largest renewable energy resources.

* Corresponding author. Tel.: +98 9121947510; fax: +98 21 88617087.
E-mail address: akasa@ut.ac.ir (A.B. Kasaeian).

http://dx.doi.org/10.1016/j.rser.2014.02.028
1364-0321

Nomenclature

C_p	Specific heat capacity (J/kg K)
g	Gravitational acceleration
h	Heat transfer coefficient (W/m^2 K)
K	incident angle modifier
κ	Thermal conductivity (W/m K)
L	Length of tube (m)
p	Pressure (Pa)
q''	Heat flux (W/m^2)
D_a	Diameter of absorber tube (m)
Re	Reynolds number
T	Temperature (K)
ΔT	Average fluid temperature above ambient air temperature(K)
u,v,w	Dimensionless velocity (m/s)
θ	Angular coordinate
r	Radial direction
μ	Dynamic viscosity (kg/m s)
ϕ	Particle volume fraction
ρ	Density (kg/m^3)
a	Absorber
bf	Base fluid
f	Focal length (m)
eff	Effective
s	Solid particle
W	Wall

The greatest advantage of the solar energy over alternative forms of fossil energy resources is that it is clean and abundant.

Although the costs of solar energy have gone down and continue to fall, the levelized costs of solar energy are still much higher than conventional energy. The levelized cost of solar concentrated power (CSP) (~194–336 USD/MW h) is four times than that of supercritical coal without carbon capture and storage (~43–88 USD/MW h) [1]. Cost is one of the major factors inhibiting development of trough collectors. Increasing the efficiency of the solar collector systems can in part alleviate this problem. Many attempts have been made to improve the performance of these systems [2–5].

Heat transfer can be enhanced by increasing the thermal conductivity of the heat transfer fluid (HTF). Thermal conductivity of metallic particles, metallic oxides and nanotubes is relatively higher than that of liquids. Addition of fine particles into heat transfer fluids (thus forming nanofluids) can significantly increase the heat transfer rate [6–8]. It is obvious that the researches on the applications of nanofluids have been popularized during the recent years. Many studies have been carried out on the effect of nanofluids and nanofluid size on heat transfer [9–10]. A number of investigations show the improvement of convection heat transfer using nanofluid. Choi et al. [11] studied engine oil/carbon nanotube nanofluids. They observed 160% enhancement of thermal conductivity using 1% volume carbon nanotube. The concentration of nanoparticles has high effects on the fluid convection heat transfer coefficient [12]. Akbari and Behzadmehr [13] investigated the mixed convection heat transfer of a water/Al_2O_3 nanofluid system in a horizontal tube with uniform heat flux. Their results demonstrate that the convective heat transfer coefficient is increased from 9% to 15% using 2% and 4% volume Al_2O_3 nanoparticles, respectively. Duangthongsuk and Wongwises [14] studied a system of water nanofluid consisting 0.2% volume TiO_2 nanoparticles which caused 6–11% enhancement of heat transfer coefficient.

Teng et al. [15] surveyed the changes in heat transfer of Al_2O_3–water nanofluid at different diameter sizes of nanoparticles. They declared better thermal conductivity in the smaller nanoparticle diameters. In another study, Heris et al. [16] compared the heat transfer performance of Al_2O_3/water with CuO/water nanofluids. They observed that the obtained heat transfer enhancement with Al_2O_3 nanoparticles is higher than that of CuO nanoparticles. As an example, they stated that at a Peclet number of 5000, the heat transfer coefficient enhancement ratio was 1.29 for 2.5% volume of Al_2O_3 nanoparticles whereas it was 1.23 for CuO/water nanofluid for the same particle volume fraction. Bianco et al. [17] considered a laminar flow of Al_2O_3/water nanofluid. Under constant wall heat flux boundary conditions, they analyzed the heat transfer of nanofluid using both single phase and two-phase approaches. They noted that the difference between the results of single phase and two-phase approaches is small, especially when the temperature dependency of the thermo-physical properties is taken into account.

Using nanofluid as a working fluid in solar systems is a novel approach to increase the efficiency of solar systems. Lenert and Wang [18] studied the influence of different variations in nanofluid volumetric receivers both theoretically and experimentally. In their theoretical part, a one-dimensional transient heat transfer model was supposed and the enhancement of receiver efficiency with augmentation of nanofluid height (H) and incident solar flux was proved. In the experimental part, carbon coated cobalt nanoparticles were added to Therminol® VP-1 in a liquid-based volumetric receiver. They illustrated that the efficiency of nanofluid volumetric receivers is increased with increasing solar concentration and nanofluid height. Also, they stated that the receiver-side efficiencies are predicted to exceed 35% when nanofluid volumetric receivers are coupled to a power cycle and optimized with respect to the optical thickness and solar exposure time. Lu et al. [19] evaluated the influence of water-based CuO nanofluids upon an open thermo syphon utilizing in a high-temperature evacuated tabular solar collector (HTC). Compared to water, nanofluid improved the thermal performance of the evaporator; also a 30% enhancement was observed for the evaporating heat transfer coefficient.

Yousefi et al. [20] investigated the effect of Al_2O_3–H_2O nanofluid on the efficiency of a flat-plate solar collector experimentally. In comparison with pure water, they declared 28.3% enhancement of efficiency for 0.2 wt% nanoparticle concentration. Also they showed that utilizing MWCNT–H_2O nanofluid enhanced the efficiency of a flat-plate solar collector [21]. Khullar et al. [22] studied the nanofluid usage in a concentrating parabolic solar collector theoretically and compared the results with the experimental data of the conventional concentrating parabolic solar collectors. Their results demonstrate 5–10% higher efficiency as compared to the conventional models. Kasaeian et al. [23] investigated the heat transfer enhancement for Al_2O_3/synthetic oil nanofluid in a parabolic trough collector tube numerically. Their results show that the heat transfer coefficient is increased as the concentration of the nanoparticles in the base fluid is increased. Otanicar et al. [24] examined the effect of different nanofluids (carbon nanotubes, graphite and silver) on the performance of a direct absorption collector. The efficiency rose with the enhancement of particles concentration but, after a volume fraction of 5%, the efficiency diminished slightly. Since the nanofluid receiver can potentially be either useful in a direct steam generation system (DSG), some works are reported in the literature [25].

Table 1
Economic comparisons for conventional and nanofluid-based solar collectors [26].

Parameter	Conventional solar collector ($)	Nanofluid solar collector ($)
Capital cost		
Independent costs	200	200
Area based costs	397.8	327.8
Nanoparticles		188.79
Total capital (one time cost)	597.8	716.59
Total maintenance (for 15 year life)	96.23	115.35
Total cost	694.03	831.94
Electricity cost saving per year	270.13	278.95
Years until electricity saving = cost	2.57	2.98
Natural gas cost saving per year	80.37	83.02
Years until natural gas saving = cost	8.64	10.02
Electricity price		
November–March (per kW h)	0.08	0.08
May–October (per kW h)	0.09	0.09
Daily service charge	0.25	0.25
Gas price rate (per term)	0.74	0.74
Monthly service charge	9.70	9.70

The use of nanofluids in solar systems is desired to be evaluated in the economic point of view. Otanicar and Golden [26] compared the economic features of nanofluid-based solar collectors with the conventional types. The study was based on life cycle assessment which is a capable methodology to evaluate the economic impacts of products. As it is shown in Table 1, the capital and maintenance costs are $120 and $20 higher for nanofluid-based collectors respectively for the year life time. The payback period is less for the conventional collectors, but with assuming 15 years life time according to the better performance of nanofluid-based collectors, the life cycle savings would be nearly the same. Taylor et al. [25] evaluated the utilization of nanofluid receivers for a solar thermal power plant theoretically. They appraised the amount of nanoparticles that would be needed for a solar thermal power plant (3 kg per each 1 MWe) and with assuming the price of nanoparticles ~$1000/kg, the total capital investment would be $5/W where the cost rise is less than 0.1% of the total capital investments. They proposed two conceptual designs for nanofluid receivers that substitute the conventional models in the solar plant which are cheaper than the conventional ceramic receivers. They used graphite/therminol® VP-1 nanofluid in the model with a volume fraction less than 0.001%. The conservative calculations exhibited that for a 100 MWe power tower solar plant operating in Tucson-Arizona, more than about $3.5 million was obtained in the yearly revenue and the payback time of the plant reduces about two years.

The objective of the current research is to model a trough collector absorber tube and study the effects of nanoparticle concentration on the mixed convection heat transfer rate of the nano-fluid in a fully developed turbulent flow. Most of the models, in the literature, for simulating the flow in a trough collector absorber tube assume that the solar flux is uniform and many correlations in the models are based on a uniform temperature. Because of the non-uniform nature of the solar flux on the outer surface of the inner absorber tube, the temperature distribution of the heat transfer fluid is, in fact, asymmetric. Relatively few investigations have been reported on simulating non-uniform heat flux in absorber tubes [27,28]. Al_2O_3/synthetic oil was used as the heat transfer fluid. The fluid properties are strongly dependent on the absorber operational temperature. The heat transfer coefficients for various volumetric concentrations of nanoparticles in the heat transfer fluid are presented along the axial and circumferential directions for a number of absorber tube operational temperatures.

2. Fluid properties

Thermo-physical properties of the base fluid (synthetic oil) and the nanoparticles (Al_2O_3) including density, viscosity, thermal conductivity, and specific heat are strongly dependent on the operational temperature. The variation of density of the base fluid with temperature was extracted from Ref. [29] and plotted in Fig. 1(a). The distributions of viscosity, thermal conductivity, and specific heat of the base fluid as a function of temperature were also obtained from [27] and used in the current study (Fig. 1(b) and (c)). Also, the properties of Al_2O_3 were taken from Ref. [30]. Addition of nanoparticles remarkably alters the thermo-physical properties of the heat transfer fluid. These properties were calculated for various concentrations of nanoparticles in the fluid and plotted in the same figure for compassion. Table A1 of Appendix A provides the numerical values of these properties for the operational temperatures of 300 K, 400 K, and 500 K. The thermo-physical properties of the base fluid, nanoparticles and nanofluid as a function of temperature are provided in Appendix A.

3. Numerical modeling

The flow of heat transfer fluid through an LS-2 parabolic trough collector module, tested on the AZTRAK rotating test platform at SNL by Dudley et al. [31], was numerically simulated. A schematic diagram of the collector and absorber tube is shown in Fig. 2 and the geometric characteristics of the collector are shown in Table 2. The absorber tube is 7.8 m (L) long and 0.07 m (D_a) in diameter. Al_2O_3/synthetic oil was used as the working fluid in the collector field and the nanofluid flow was modeled as single phase. Since the Re is higher than 2500 and Richardson number ($Ri = Gr/Re^2$) is between 0.1 and 10, the flow is assumed to be fully developed turbulent mixed convection. Gravitational acceleration was also taken into account. The operational temperatures are 300 K, 400 K, and 500 K and the pressure is assumed 20 psig. The fluid motion governing equations were solved using the FLUENT software. The governing equations are provided in Appendix A.

A k–ε formulation was used to model the turbulence in the flow. In the k–ε model, the turbulence characteristics are described based on the turbulent kinetic energy (TKE) and viscous dissipation of turbulent kinetic energy. The FLUENT software was used to numerically simulate the flow of the nano-fluid in the absorber tube. This software is based on finite volume method. To couple the velocity field and pressure, the SIMPLE model was employed. In this method, the pressure correction equation is solved in a number of iterations, and then the velocity is corrected until the continuity equation is satisfied in the computational domain. For the convective and diffusive terms, a second order discretization method was used. The flow was assumed three-dimensional, steady state, and single-phase. To insure that the results were time independent, the average heat transfer coefficient was monitored with the size of the grid.

The solar energy flux distribution on the outer wall of the inner absorber tube was obtained using the Monte Carlo Ray Trace (MCRT) technique developed by He et al. [27]. The heat flux distribution of He et al. (Fig. 3) was used in the current study. In the numerical simulations, the boundary condition on the absorber tube wall was set to this non-uniform heat flux distribution

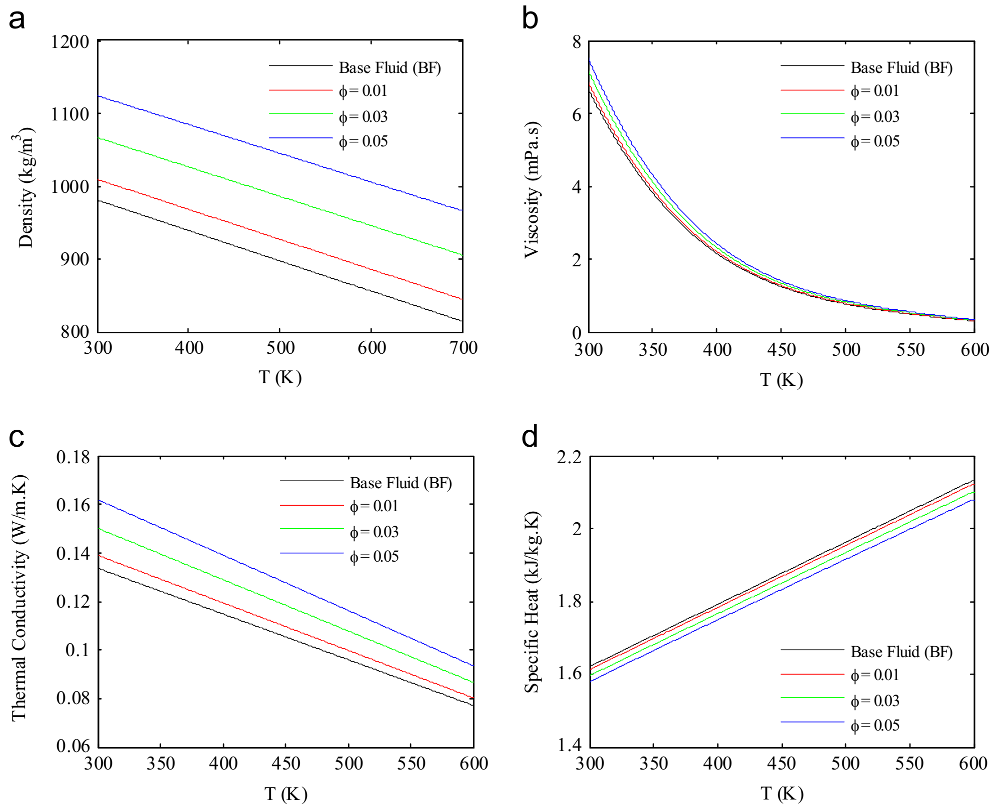


Fig. 1. (a) Density, (b) viscosity, (c) thermal conductivity, and (d) specific heat of the base fluid as well as the nanofluid for various particle concentrations at different operational temperatures.

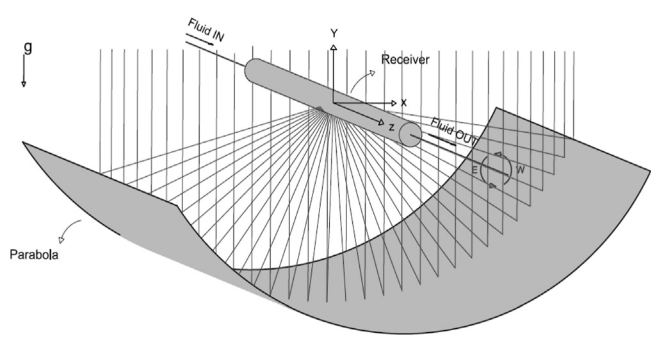


Fig. 2. Schematic diagram of the parabolic trough collector and absorber tube. Red lines represent rays of light from the Sun. (For interpretation of the references to color in this figure caption, the reader is referred to the web version of this article.)

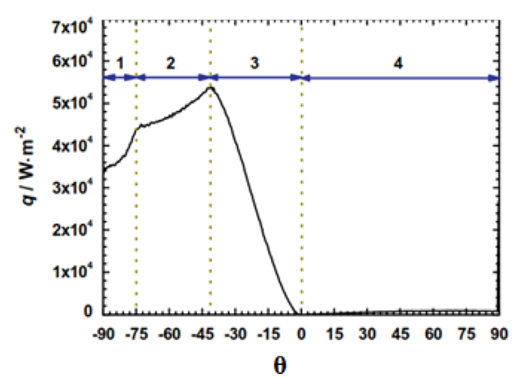


Fig. 3. Heat flux distribution of the absorber tube as a function of angle. Graph was reproduced from [27].

Table 2
Specifications of the LS-2 parabolic trough collector [31].

System Type	Parameter	Value
Parabolic trough reflector	$Z_L{*}X_L$	7.8 m*5 m
	f	1.84 m
Receiver	r_g	0.0575
	r_a	0.035

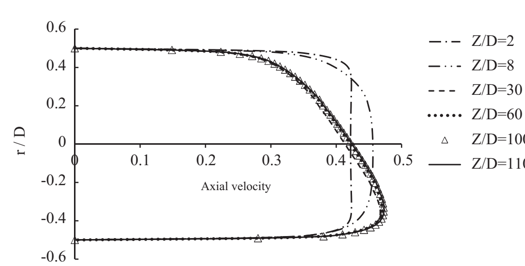


Fig. 4. Axial velocity profiles at different axial positions at Re=26 000.

using a user-defined function in the FLUENT software. In addition, the boundary conditions at the inlet ($z=0$) were as

$$w=w_0, \quad u=v=0, \quad T=T_i$$

where u, v, and w are the velocity components in x, y, and z directions, respectively, and T is the temperature of the fluid. The flow at the outlet of the tube was assumed fully developed and an outflow condition was used in the simulations, the fully developed entrance length is demonstrated in Appendix A. Also, Fig. 4 shows the axial velocity profiles at six different cross sections for a given Re (260 00). We can observe that the fully developed region occurs in $Z/D=30$.

Furthermore, the following boundary conditions were used at the fluid–solid interface:

$$u = v = w = 0, \quad q'' = -\kappa_{eff}\frac{\partial T}{\partial r}$$

The MCRT method is dependent on the geometric (r, Z_L) as well as the grid (N_c, N_z) parameters. The MCRT method requires a grid density for the absorber tube of $N_c > 68$ and $N_z > 320$. A structured non-uniform mesh was created to discretize the computational domain. It is finer near the wall where the velocity and temperature gradients are larger. The standard method to test for grid independence is to increase the resolution and repeat the simulation. If the results do not change appreciably, the original grid is probably adequate and the results are not dependent on the girds size. If, on the other hand, there are significant differences between the two solutions, the original grid is likely of inadequate resolution. In such a case, an even finer grid should be tried until the grid is adequately resolved. A number of grid sizes were studied to insure that the accuracy of the results is independent of the grid size. The mean heat transfer coefficient was monitored for two cases: (1) $T=500$ K and $\varphi=0$ and (2) $T=500$ K and $\varphi=0.05$. The results of the grid refinement study are presented in Table 3. Increasing the grid numbers does not significantly change the mean heat transfer coefficient. The final mesh for the current study consisted of 68 (N_c), 320 (N_z), and 20 (N_r) nodes in the circumferential, axial and radial directions, respectively.

Table 3
Average heat transfer coefficients at 500 K for various grid sizes.

Grid ($N_c^* N_r^* N_z$)	Mean heat transfer coefficient at $\phi=0$	Mean heat transfer coefficient at $\phi=0.05$
68–20–320	137.99	146.53
68–30–400	137.75	147.01
80–20–480	138.01	146.55

4. Validation

Two available experimental cases were used to validate the current numerical study.

4.1. LS-2 solar collector

Three typical states for a bare tube from Dudley et al.'s report [31] were used for the purpose of validation. The results are presented in Table 4. Dudley et al. derived the performance correlation between the collector efficiency and the working fluid temperature as following [31]:

$$\eta = K*(73.3 - 0.007276*\Delta T) + \left(4.96*\left(\frac{\Delta T}{I_b}\right)\right) - 0.0691*\left(\frac{(\Delta T)^2}{I_b}\right)$$

In the equation, K is the incident angle modifier and may be assumed to be one ($K=1$).

The heat flux distribution on the outer surface of absorber tube is shown in Fig. 5(a). The temperature distribution on the outer surface of absorber tube is also shown in Fig. 5(b). Fig. 5(b) shows the wall temperature distributions of the absorber tube based on the test condition state 1. Fig. 6 shows the temperature distribution in the axial direction with $\theta=0°$, 90°, 180°, 270° and 310°. The wall temperature increases with the increase of z along axial direction, and the temperature at 310° is much larger than the other angular direction. The reason is that, $\theta=310°$ is on the side with high concentrated solar radiation, while $\theta=90°$ is on the side without concentrated solar radiation. According to the simulated outlet temperature and collector efficiency based on the test results of Dudley (Table 4), the absolute error is less than 3.8 °C which has good agreement with the obtained simulation results. This proves that the models and methods used in the present study are feasible and the numerical results are reliable

Table 4
The experimental data from Dudley and comparisons with our simulation result.

Test	I_b (W/m^2)	$\dot{m}$ (kg/s)	Reynolds	T_a (°C)	T_{in} (°C)	$T_{o,test}$ (°C)	$T_{o,model}$ (°C)	E (%)	$\eta_{(test)}$ (%)	$\eta_{(model)}$ (%)
State 1	933.7	0.66	4501	21.2	102.2	124	126.1	1.69	72.51	72.27
State 2	968.2	0.65	7653	22.4	151	173.3	176.9	2.1	70.9	71.5
State 3	937.9	0.61	28560	28.8	297.8	316.9	319.32	0.76	68.98	66.9

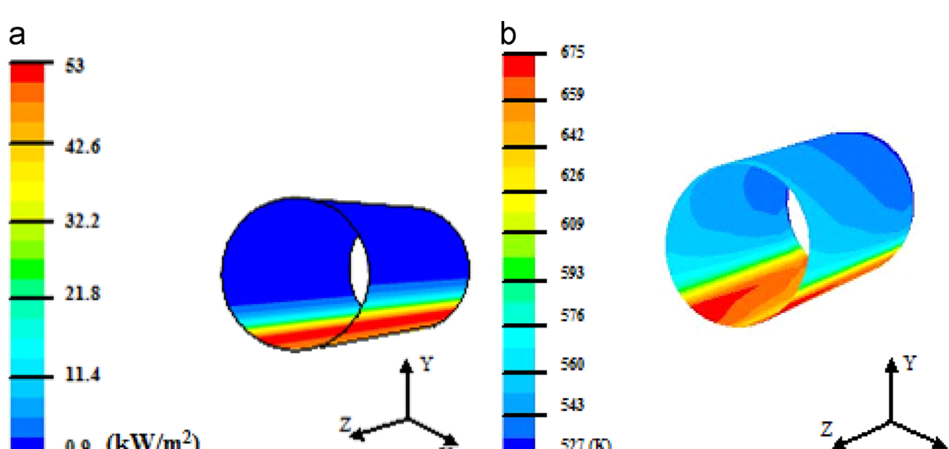


Fig. 5. (a) Heat flux and (b) temperature distributions on the outer surface of the absorber tube.

4.2. Al_2O_3 nanofluid flow through a horizontal tube

Heat transfer coefficient and Nusselt number were obtained and compared with the experimental results of Esmaeilzadeh et al. [32] in a horizontal tube. Fig. 7(a) and (b) shows the both the results of the current numerical study and those of Esmaeilzadeh et al. [32]. The axial evolution of Nusselt number and heat transfer coefficient are in good agreement with the corresponding experimental results.

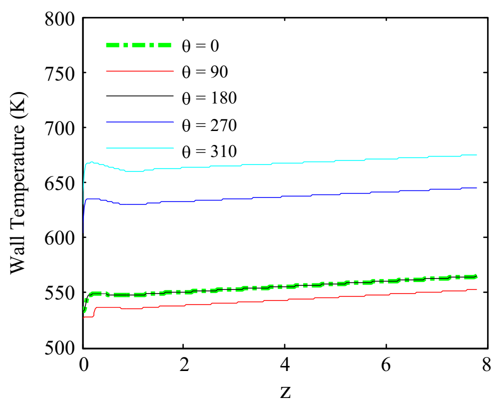


Fig. 6. Mean temperature distributions along the axial direction (z) on the outer surface of absorber tube at various angular locations at Re = 17 361.

5. Results and discussion

The study of heat transfer was carried out on a trough collector absorber tube with 7.8 m length and 0.07 m diameter. The tube is consumed to be evacuated inside the space between the absorber metal tube and the glass tube. The vacuum level in the annular space between the inner absorber tube and the outer glass cover tube is so high that the convective heat losses could be essentially eliminated, but the thermal radiation heat transfer between the outer wall of absorber tube and the inner surface of glass cover tube is taken into account. Also, the heat transfer mechanism inside the tube is as convection and the inlet fluid velocity is assumed to be 4 m/s. The convection heat transfer of nanofluid may be increased compare to the base fluid. The improved thermal conductivity of nanofluid is the most important factor for improving heat transfer in parabolic trough collectors. Actually, nanofluid reduces the thermal resistance at interfaces and minimizes the temperature difference between the absorber and the heat transfer fluid. The effects of the particle concentration on the flow fields and heat transfer coefficient along the absorber tube are presented. Convection heat transfer coefficients at various axial locations for a given Reynolds number and five volumetric concentrations of Al_2O_3 particles are shown in Fig. 8. Because of the non-uniform heat flux nature, a number of graphs are shown for heat transfer coefficients (Fig. 8). As shown, the heat transfer coefficient ranges from 100 to 260 and 60 to 160 at the operational temperatures of 300 K and 500 K, respectively, indicating the

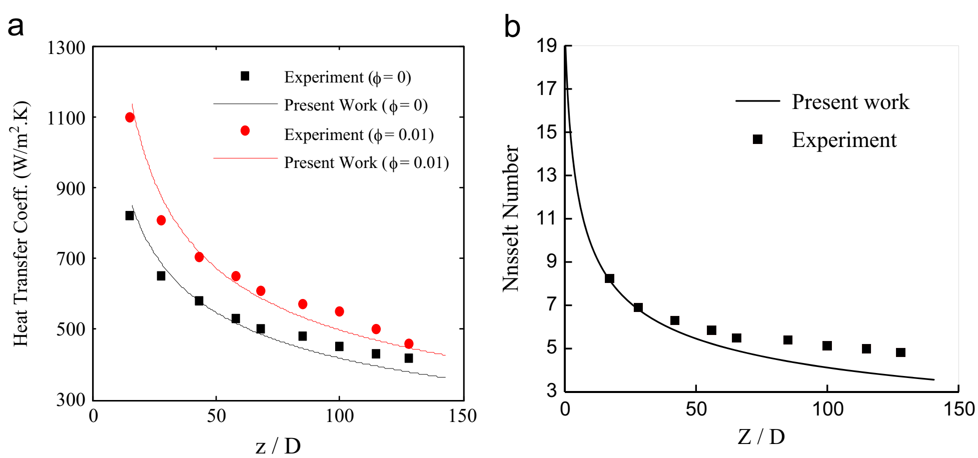


Fig. 7. Comparison of (a) the heat transfer coefficients, (b) the Nusselt number along the axial direction from the current numerical study with the existing experimental values.

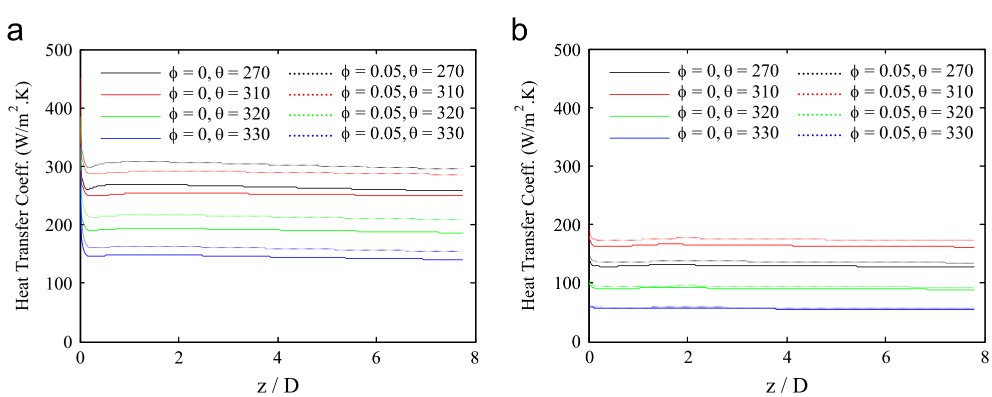


Fig. 8. Convective heat transfer coefficient vs. axial distance for various particle concentrations and angular locations for (a) Re = 3900 (T = 300 K) and (b) Re = 26 800 (T = 500 K).

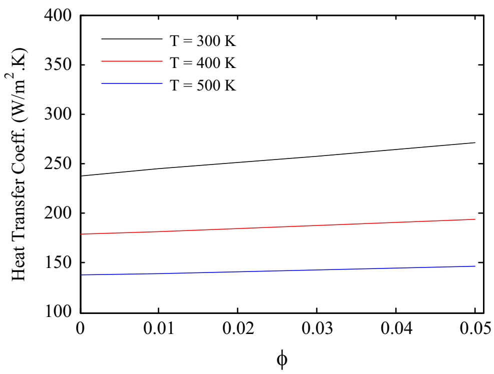


Fig. 9. Mean convective heat transfer coefficient vs. particle concentration at the operational temperatures of 300, 400 and 500 K.

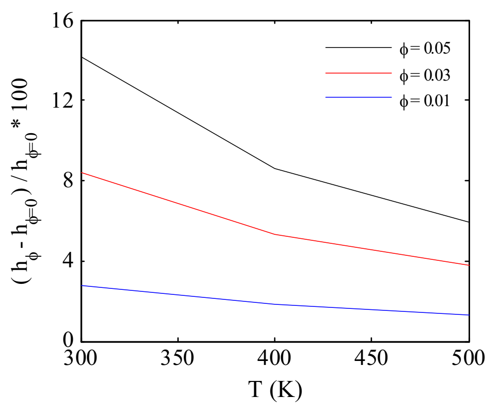


Fig. 10. Percentage increase in mean convection heat transfer coefficient due to the addition of nanoparticles to the base fluid vs. operational temperature for various particle volume concentrations.

decrease of heat transfer coefficient with the increase in operational temperature.

The heat transfer coefficient sharply drops and then levels off to its fully developed value. As the nanoparticle concentration increases, the heat transfer coefficient rises. The coefficient is more affected by the particle concentration at the operation temperature of 300 K than 500 K. However, the heat transfer coefficient is reduced as the operational temperature is increased from 300 K to 500 K. The average heat transfer coefficients are lower for the higher temperatures (Fig. 9). As shown in this figure, the average convection heat transfer coefficient increases by about 14% by increasing the nanoparticle volumetric concentration by 5% at the operational temperature of 300 K. Also, the effect of nanofluid concentrations on average heat transfer coefficient at the operational temperature of 400 K increases by 8.6% with the addition of 5% (in volume) of Al_2O_3 nanoparticles. This effect was also studied at 500 K and the results show that the average convective heat transfer coefficient increases 6% by adding 5% (in volume) of Al_2O_3 nanoparticles.

From Fig. 1, we can observe that when the operational temperature is 300 K the value of μ increases to 8.38e−4 and the value of k increase to 0.028 by adding 5 vol% of Al_2O_3 nanoparticles. While at the operational temperature of 400 K, the value of μ increases to 2.7e−4 and the value of k increase to 0.023 by adding 5 vol% of Al_2O_3 nanoparticles. Also at the operational temperature of 500 K the value of μ increases to 9.6e−5 and the value of k increases to 0.019 by adding 5 vol% of Al_2O_3 nanoparticles. The other reason for the lower increase in heat transfer coefficient at higher temperatures can be associated to the decrease in viscosity and thermal conductivity change rates at higher temperatures [23]. The percentage increase in heat transfer at various temperatures is shown in Fig. 10. According to this figure, the percentage of heat transfer increase has a descending trend with temperature rising.

6. Conclusions

The thermal behavior of a nanofluid consisting of synthetic oil and Al_2O_3 throughout a parabolic trough collector absorber tube ($L=7.8$ and $D=0.07$ m) has been simulated and a turbulent mixed convection heat transfer with non-uniform heat flux has been investigated. The results of the current study illustrate that the heat transfer coefficient of the working fluid in an absorber tube is enhanced at the presence of nanoparticles. The heat transfer coefficient is increased as the concentration of the nanoparticles in the base fluid is increased. For a given inlet Reynolds number, the enhancement in heat transfer coefficient caused by nanoparticles is decreased as the operational temperature of the absorber tube is increased. The maximum heat transfer coefficients were obtained at the left and right sides of the tube ($\theta=310$ and $\theta=230$).The results of this work for investigating the heat transfer variations of the assumed collector were validated with the other similar studies.

Utilizing nanofluid in PTC has environmental benefit and causes improving heat transfer, consequently reducing the needed heat transfer area of the tubes and heat exchangers. Nevertheless, these advantages could be achieved with little change (in terms of materials, system design, and initial capital investment) on the entire PTC system.

Appendix A

Fluid properties:

$$\rho_{bf} = -0.9985*T + 1236 \text{ kg}/m^3 \quad (1)$$

$$\rho_s = 3850 \text{ kg/m}^3 \quad (2)$$

$$\rho_{eff} = (1-\phi)\rho_{bf} + \phi\rho_s \quad (3)$$

The correlation of effective density is taken of [33]:

$$\mu_{bf} = 6.67*10^{-7}T^4 - 1.56*10^{-3}T^3 + 1.38*T^2 - 5.541*10^2T + 8.848*10^4 \ \mu\text{Pa s} \quad (4)$$

$$\mu_{eff} = (1+2.5\phi)\mu_{bf} \quad (5)$$

The correlation of effective viscosity is taken of Einstein's [34]:

$$\kappa_{bf} = -5.753496*10^{-10}T^2 - 1.875266*10^{-4}T + 1.900210*10^{-1} \text{ W/m K} \quad (6)$$

$$\kappa_s = 5.5 + 34.5*e^{(-0.0033*(T-273))} \text{ W/m K} \quad (7)$$

$$\kappa_{eff} = \kappa_f * \left[\frac{\kappa_s + 2\kappa_f - 2(1+\beta)^3\phi(\kappa_f - \kappa_s)}{\kappa_s + 2\kappa_f + (1+\beta)^3\phi(\kappa_f - \kappa_s)}\right] \quad (8)$$

where β is the ratio of nanolayer thickness to the nanoparticles diameter which is considered to be 0.1 in Eq. (8) of this study [35].

$$Cp_{bf} = 0.001708T + 1.107798 \text{ kJ/kg K} \quad (9)$$

$$Cp_s = 1.046 + 1.74*10^{-4}T - 2.79*10^4T^2 \text{ kJ/kg K} \quad (10)$$

$$(Cp)_{eff} = (1-\phi)Cp_{bf} + \phi Cp_s \quad (11)$$

The correlation of effective specific heat is taken of [33].

Table A1
Nanofluid (Al_2O_3) thermo-physical properties at 300, 400 and 500 K.

Property	T=300 K				T=400 K				T=500 K			
	0	1%	3%	5%	0	1%	3%	5%	0	1%	3%	5%
ρ (kg/m^3)	936.5	965.6	1023.9	1082.1	836.6	866.7	927.0	987.3	736.7	766.9	830.1	892.4
Cp (J/kg K)	1620	1612	1595	1578	1791	1782	1765	1748	1962	1952	1934	1915
K (W/m K)	0.134	0.139	0.150	0.161	0.115	0.119	0.129	0.138	0.096	0.100	0.107	0.115
μ (mPa s)	6.68	6.84	7.18	7.518	2.16	2.22	2.33	2.43	0.77	0.789	0.828	0.866

In all of the correlations *f*, *s* and *eff* correspond to the based fluid, nanoparticle and nanofluid, respectively and ϕ is the volumetric concentration of Al_2O_3 in the nano-fluid. The thermo-physical properties of the nanofluid were calculated via (3), (5), (8), (11). The governing equations for the fluid motion in a cylindrical coordinate system are described as follows:

Continuity equation:

$$\frac{1}{r}\frac{\partial}{\partial\theta}(\rho_{eff}u)+\frac{1}{r}\frac{\partial}{\partial r}(\rho_{eff}rv)+\frac{\partial}{\partial Z}(\rho_{eff}w)=0 \tag{12}$$

Momentum equation:

θ component:

$$\begin{aligned}&\frac{1}{r}\frac{\partial}{\partial\theta}(\rho_{eff}uu)+\frac{1}{r}\frac{\partial}{\partial r}(\rho_{eff}rvu)+\frac{\partial}{\partial Z}(\rho_{eff}wu)+\frac{1}{r}(\rho_{eff}uv)\\&\quad=-\frac{1}{r}\left(\frac{\partial p}{\partial\theta}\right)+\frac{1}{r^2}\frac{\partial}{\partial\theta}\left(\mu_{eff}\frac{\partial u}{\partial\theta}\right)+\frac{\partial}{\partial r}\left(\frac{\mu_{eff}}{r}\frac{\partial(ru)}{\partial r}\right)\\&\quad\quad+\frac{2\mu_{eff}}{r^2}\frac{\partial v}{\partial\theta}+\rho_{eff}g\beta_{eff}(T_W-T)\sin\ \theta\end{aligned} \tag{13}$$

r component:

$$\begin{aligned}&\frac{1}{r}\frac{\partial}{\partial\theta}(\rho_{nf}uv)+\frac{1}{r}\frac{\partial}{\partial r}(\rho_{nf}rvv)+\frac{\partial}{\partial Z}(\rho_{nf}wv)-\frac{1}{r}(\rho_{nf}u^2)\\&\quad=-\frac{1}{r}\left(\frac{\partial p}{\partial r}\right)+\frac{1}{r^2}\frac{\partial}{\partial\theta}\left(\mu_{nf}\frac{\partial v}{\partial\theta}\right)+\frac{\partial}{\partial r}\left(\frac{\mu_{nf}}{r}\frac{\partial(rv)}{\partial r}\right)\\&\quad\quad-\frac{2\mu_{nf}}{r^2}\frac{\partial u}{\partial\theta}-\rho_{nf}g\beta_{nf}(T_W-T)\cos\ \theta\end{aligned} \tag{14}$$

Z component:

$$\begin{aligned}&\frac{1}{r}\frac{\partial}{\partial\theta}(\rho_{eff}uw)+\frac{1}{r}\frac{\partial}{\partial r}(\rho_{eff}rvw)+\frac{\partial}{\partial Z}(\rho_{eff}w^2)\\&\quad=-\frac{\partial p}{\partial Z}+\frac{1}{r^2}\frac{\partial}{\partial\theta}\left(\mu_{eff}\frac{\partial w}{\partial\theta}\right)+\frac{1}{r}\frac{\partial}{\partial r}\left(r\mu_{eff}\frac{\partial w}{\partial r}\right)\end{aligned} \tag{15}$$

Energy equation:

$$\begin{aligned}&\frac{1}{r}\frac{\partial}{\partial\theta}(\rho_{eff}uT)+\frac{1}{r}\frac{\partial}{\partial r}(\rho_{eff}rvT)+\frac{\partial}{\partial Z}(\rho_{eff}wT)\\&\quad=\frac{1}{r^2}\frac{\partial}{\partial\theta}\left(\frac{\kappa_{eff}}{(Cp)_{eff}}\frac{\partial T}{\partial\theta}\right)+\frac{\partial}{r\partial r}\left(r\frac{\kappa_{eff}}{(Cp)_{eff}}\frac{\partial T}{\partial r}\right)\end{aligned} \tag{16}$$

where *r*, θ, and *z* are the coordinates, *u*, *v*, and *w* are the velocity components and *p*, *T* and *g* are the pressure, temperature and gravitational acceleration. ρ, *k*, μ, and C_p are the effective density, thermal conductivity, dynamic viscosity and specific heat capacity of the nano-fluid.

The fully developed entrance length:

$1.22 < L_h = (4.4{*}\mathrm{Re}^{1/6}){*}D < 1.$
$6L_{t\,=}\ 10{*}D = 0.7$ m

See Table A1.

References

[1] Timilsina GR, Kurdgelashvili L, Narbel PA, A review of solar energy markets, economics and policies. Policy Research Working Paper; 2011.
[2] Xiaowu W, Ben H. Exergy analysis of domestic-scale solar water heaters. Renew Sustain Energy Rev 2005;9(6):638–45.
[3] Wang X, Wang R, Wu J. Experimental investigation of a new-style double-tube heat exchanger for heating crude oil using solar hot water. Appl Therm Eng 2005;25(11–12):1753–63.
[4] Al-Madani H. The performance of a cylindrical solar water heater. Renew Energy 2006;31(11):1751–63.
[5] Ho CD, Chen TC. The recycle effect on the collector efficiency improvement of double-pass sheet-and-tube solar water heaters with external recycle. Renew Energy 2006;31(7):953–70.
[6] Eric DK. Engines of creation. 4th edition. London: Oxford Press; 1986.
[7] Maxwell JC, A treatise on electricity and magnetism, vol. 1. UK: Oxford.
[8] Terekhov VI, Kalinina SV, Lemanov VV. The mechanism of heat transfer in nanofluids: state of the art (review). Part 2. Convective heat transfer. Thermophys Aeromech 2010;17(2):157–71.
[9] Moraveji MK, Darabi M, Haddad SMH, Davarnejad R. Modeling of convective heat transfer of a nanofluid in the developing region of tube flow with computational fluid dynamics. Int Commun Heat Mass Transfer 2011;38(9): 1291–1295.
[10] Nguyen C, Desgranges F, Roy G, Galanis N, Maré T, Boucher S, et al. Temperature and particle-size dependent viscosity data for water-based nanofluids - hysteresis phenomenon. Int J Heat Fluid Flow 2007;28(6):1492–506.
[11] Choi SUS, Zhang ZG, Yu W, Lockwood FE, Grulke EA. Anomalous thermal conductivity enhancement in nanotube suspensions. Appl Phys Lett 2001; 79(14):2252–4.
[12] Tsai CY, Chiena HT, Dingb PP, Chanc B, Luhd TY, Chena PH. Effect of structural character of gold nanoparticles in nanofluid on heat pipe thermal performance. Mater Lett 2004;58(9):1461–5.
[13] Akbari M, Behzadmehr A. Developing mixed convectionof a nanofluid in a horizontal tube with uniform heat flux. Numer Methods Heat Fluid Flow 2006;17(6):566–86.
[14] Duangthongsuk W, Wongwises S. Heat transfer enhancement and pressure drop characteristics of TiO2–water nanofluid in a double-tube counter flow heat exchanger. Int J Heat Mass Transf 2009;52(7–8):2059–67.
[15] Teng T-P, Hung Yi-H, Teng T-C, Mo H-E, Hsu H-G. The effect of alumina/water nanofluid particle size on thermal conductivity. Appl Therm Eng 2010; 30(14–15):2213–8.
[16] Zeinali Heris S, Etemad SG, Esfahany M Nasr. Experimental investigation of oxide nanofluids laminar flow convective heat transfer. Int Commun Heat Mass Transf 2006;33(4):529–35.
[17] Bianco V, Chiacchio F, Manca O, Nardini S. Numerical investigation of nanofluids forced convection in circular tubes. Appl Therm Eng 2009; 29(17–18):3632–42.
[18] Lenert A, Wang EN. Optimization of nanofluid volumetric receivers for solar thermal energy conversion. Sol Energy 2012;86(1):253–65.
[19] Lu L, Liu Z-H, Xiao H-S. Thermal performance of an open thermosyphon using nanofluids for high-temperature evacuated tubular solar collectors: Part 1: Indoor experiment. Sol Energy 2011;85(2):379–87.
[20] Yousefi T, Veysi F, Shojaeizadeh E, Zinadini S. An experimental investigation on the effect of Al_2O_3–H_2O nanofluid on the efficiency of flat-plate solar collectors. Renew Energy 2012;39(1):293–8.
[21] Yousefi T, EhsanShojaeizadeh E, SirusZinadini S. An experimental investigation on the effect of MWCNT-H_2O nanofluid on the efficiency of flat-plate solar collectors. Exp Therm Fluid Sci 2012;39(0):207–12.
[22] Khullar V, Tyagi H, Patrick E, Phelan PE, Otanicar T, Singh H, et al. Solar energy harvesting using nanofluids-based concentrating solar collector. J Nanotechnol Eng Med 2012;3(3): (031003-031003-9).
[23] Kasaeian AB, Sokhansefat T, Abbaspour MJ, Sokhansefat M. Numerical study of heat transfer enhancementby using Al_2O_3/synthetic oil nanofluid in aparabolic trough collector tube, Rome: World Academy of Science, Engineering and Technology; 2012. p. 1154–9.
[24] Otanicar T, Phelan PE, Prasher RS, Rosengarten G, Taylor RA. Nanofluid-based direct absorption solar collector. Renew Sustain Energy 2010;2:033102.
[25] Taylor RA, et al. Applicability of nanofluids in high flux solar collectors. J Renew Sustain Energy 2011;3:023104.
[26] Otanicar TP, Golden JS. Comparative environmental and economic analysis of conventional and nanofluid solar hot water technologies. Environ Sci Technol 2009;43(15):6082–7.

[27] He Y-L, Xiao J, Cheng Z-D, Tao Y-B. A MCRT, FVM coupled simulation method for energy conversion process in parabolic trough solar collector. Renewable Energy 2011;36(3):976.
[28] Cheng ZD, He YL, Xiao J, Tao YB, Xu RJ. Three-dimensional numerical study of heat transfer characteristics in the receiver tube of parabolic trough solar collector. Int Communi Heat Mass Transfer 2010;37(7):782–7.
[29] SYLTERM 800 heat transfer fluid; 1997. Dow Chemical Company.
[30] Auerkari P. Mechanical and physical properties of engineering alumina ceramics. VTT Manufacturing Technology Technical Research Center of Finland; 1792.
[31] Dudley VE, kolb GJ, Sloan M, Kearney D. Segs Ls2 solar collector-test results. Sandia: Sandia Natinal Laboratories; 1994.
[32] Esmaeilzadeh E, Almohammadi H, NasiriVatan Sh, Omrani AN. Experimental investigation of hydrodynamics and heat transfer characteristics of Î³-Al_2O_3/water under laminar flow inside a horizontal tube. Int J Therm Sciences 2013;63(0):31–7.
[33] Ayatollahi M, Nasiri SH, Kasaeian AB. Convection heat transfer modeling of Ag nanofluid using different viscosity theories. IIUM Eng J 2012;13(1).
[34] Einstein A, Investigation on the theory of Brownian motion; 1926.
[35] Yu W, Choi SUS. The role of interfacial layers in the enhanced thermal conductivity of nanofluids: a renovated Hamilton–Crosser model. J Nanopart Res 2004;6(4):355–61.